Structures of Large T Antigen at the Origin of SV40 DNA Replication by Atomic Force Microscopy

Iris A. Mastrangelo,* Magdalena Bezanilla,‡ Paul K. Hansma,‡ Paul V. C. Hough,* and Helen G. Hansma‡
*Biology Department, Brookhaven National Laboratory, Upton, New York 11973, and ‡Department of Physics, University of California, Santa Barbara, California 93106 USA

ABSTRACT For inorganic crystals such as calcite ($CaCO_3$), Atomic Force Microscopy (AFM) has provided surface structure at atomic resolution (Ohnesorge and Binnig, 1993). As part of a broad effort to obtain high resolution for an individual protein or protein assembly (Binnig et al., 1986; Rugar and Hansma, 1990; Radmacher et al., 1992), we applied AFM to study the ATP-dependent double hexamer of SV40 large T antigen, which assembles around the viral origin of DNA replication. Multimeric mass has been determined in two-dimensional projected images by Scanning Transmission Electron Microscopy (STEM) (Mastrangelo et al., 1989). By AFM, if the DNA-protein preparation has been stained positively by uranyl acetate, the contour at the junction between hexamers is visible as a cleft, 2–4 nm deep. The cleft, whether determined as a fraction of height by AFM or as a fraction of mass thickness by STEM, is of comparable magnitude. On either side of the cleft, hexamers attain a maximum height of 13–16 nm. Monomers found in the absence of ATP show heights of 5–7 nm. Taken together, the z coordinates provide a surface profile of complete and partial replication assemblies consistent with the spatial distribution of recognition pentanucleotides on the DNA, and they contribute direct geometrical evidence for a ring-like hexamer structure.

INTRODUCTION

Simian virus 40 large T antigen binds as a double hexamer at the viral origin of DNA replication to destabilize the helix as an ATP-dependent initial step in replication (Borowiec et al., 1990). Besides DNA recognition and helicase functions, it interacts specifically with eukaryotic cellular replication proteins, DNA polymerase α-primase and RF-A single-strand binding protein (Fanning and Knippers, 1992). Further, large T antigen promotes cellular transformation via specific interactions that sequester tumor suppressor proteins, p53 and the retinoblastoma (RB) gene product (Weinberg, 1991). These functions have been shown to reside in separate protein-sequence domains through mutational and biochemical analyses, but their spatial locations are largely unknown. We have imaged the double hexamer at origin DNA by Atomic Force Microscopy (AFM) and observed maximal protein heights differing by 10 nm for assembly in the presence and absence of ATP. Combining simple specimen preparation procedures used in STEM, conventional transmission EM (TEM), and AFM, height measurements were achieved in a routine and reproducible manner. These first topographical images of the replication assembly and its monomer subunits confirm a likely model for the quaternary structure and open the way to study of functional domains and their multiple molecular interactions.

MATERIALS AND METHODS

Binding reactions and sample preparation

Purification of baculovirus-expressed T antigen and preparation of pOR1 DNA and binding reactions, with and without ATP, were as described previously (Mastrangelo et al., 1989). After incubation for binding at 37°C for 1 h, the buffer was brought to 0.1% in glutaraldehyde, and incubation continued for 15 min. Unbound protein was separated from DNA by passing reactions through Sepharose 4B (Pharmacia, Piscataway, NJ) minicolumns. For AFM, 0.2 μl from void volume fractions was placed on a freshly cleaved mica disc. DNA concentrations in the fractions used varied between 0.5 and 1 ng per μl. Others have reported treating mica to improve DNA adhesion and spreading (Bustamante et al., 1992; Hansma et al., 1992; Lyubchenko et al., 1992). We found that 200 pg of DNA applied to an untreated mica surface in the STEM postreaction column buffer (40 mM HEPES/KOH, pH 7.7, 10 mM $MgCl_2$) (Mastrangelo et al., 1989) provided abundant and readily controllable concentrations of securely anchored DNAs. After application to mica, the column fraction droplet was washed with 3 drops of Milli-Q-purified water. Tipping mica onto Whatman 541 filter paper removed most of the wash water. While still moist, 0.5 μl of 5% aqueous uranyl acetate was added for 15 s, washed with water, and removed. Filtered, compressed air dried the mica surface. Storage for several h in a dessicator jar evacuated to 30 millitorr and containing phosphorous pentoxide preceded viewing.

AFM Imaging

Data were collected on a Digital Instruments Nanoscope II AFM (Santa Barbara, CA) run at constant force, in the height mode, at a scan speed of 8.7 Hz, or 45 s/image. One-μm fields were scanned in both y directions and at 0° and 90°. Nanoprobe 200 μm, "wide" cantilevers with oxide-sharpened integral tips were used. At the time of data collection, calibration readings on microfabricated test specimens indicated an absolute error in height measurement of less than 10%. Lateral dimensions were calibrated by a precision grating.

For the quantitative perspective views of Figs. 2 and 3 the Z range of 30 or 32 nm has been divided into 10 hues (cycles of violet-blue-green-yellow-orange-red, above white for the mica). Each hue represents 1.5 nm of height. DNA as scanned is normally continuous (see Fig. 1).

RESULTS

Large T antigen was incubated for binding with a linearized plasmid, pOR1, containing the 64-bp sequence comprising the core origin of replication (Fig. 1 *c*). Binding in

Received for publication 12 August 1993 and in final form 4 November 1993.
Address reprint requests to Iris A. Mastrangelo and Helen G. Hansma.

0006-3495/94/02/293/06 $2.00

the absence of ATP is known to occur as individual 85-kDa monomers at four 5′-GAGGC-3′ recognition sites separated center-to-center by 6 bp (Tjian, 1979; DeLucia et al., 1983; Mastrangelo et al., 1985). The sites are part of a 27-bp exact palindrome centered on the origin. In the presence of ATP, binding affinity increases 10-fold (Deb and Tegtmeyer, 1987; Borowiec and Hurwitz, 1988a) and hexamers assemble, one hexamer surrounding each half of the palindrome.

Large, bilobed protein structures were observed at the origin sequence by TEM (Dean et al., 1987) and STEM. Similar structures are imaged by AFM in dry N_2 and are shown in Fig. 1, *a* and *b*. Observed T-antigen assemblies are bound specifically at the replication origin, on well spread, highly visible DNA whose measured length is 4% shorter than predicted for form B-DNA (Table 1). Our measured DNA lengths by STEM are comparable, and by TEM, using stain and shadow, typically are 5–7% shorter than form B. Structural features observed in the T antigen/origin DNA complexes described here extend advances recently made in visualizing DNA and DNA-bound proteins by AFM (Bustamante et al., 1992; Hansma et al., 1992; Lyubchenko et al., 1992; Zenhausern et al., 1992; Murray et al., 1993; Rees et al., 1993; Samori et al., 1993; Shaiu et al., 1993).

The AFM images shown in Figs. 1–3 are stable on repeated scanning in 1-μm fields, but on rescanning at a smaller field size they often show damage to the protein. In the absence of uranyl acetate stain (see Materials and Methods), tip damage to protein was severe at all field sizes used, from 100 to 2000 nm. This standard treatment from TEM was introduced first to increase the visibility of DNA. In stain + metal-shadow preparation of DNA for TEM, it is known that if uranyl acetate is omitted, metal shadowing produces much less contrast. The effect suggests that attachment of uranyl ionic complexes to DNA phosphate groups (Hayat, 1980) prevents z collapse of DNA. In the present experiments, staining with uranyl acetate is found to increase the measured DNA height in dry N_2 from 0.5 ± 0.1 to 1.1 ± 0.2 nm (n = 50), which is comparable to the best routine heights achieved when viewing unstained DNA under propanol with special supertips (Hansma et al., 1992). Similarly, attachment of uranyl ionic complexes to ligands, such as carboxyl residues, at the protein surface appears to preserve quaternary structure. In a dry N_2 environment, we regularly measured imaging forces between 2 and 7 nN, indicating relatively little adhesion to the surfaces scanned.

The two z-coordinate peaks in the AFM micrographs of Fig. 2, *a–c* and in structures not shown, are the highest structures observed by AFM and are believed to be double hexamers, as demonstrated in STEM by mass measurement. For comparison, Fig. 2 *f* reproduces a STEM micrograph of the T-antigen double hexamer at 1.3 times AFM magnification. Evidently, DNA by AFM at 1.1-nm height on mica is in most cases continuous, whereas the scattered-electron-count images on carbon foil by STEM are gapped, an effect known to result from statistical fluctuations. The AFM maximal structures rise between 13 and 16 nm above the mica surface (Table 1, (6+6) mer). In Figure 2, *a–c*, and in the 5 other maximal structures not shown, a lateral separation of 12 to 14 nm between peaks compares well with 12-nm separation between centers of maximum mass thickness observed by STEM. In six of eight assemblies, clefts 2 to 4 nm deep lie between hexamer peaks. This is likely to be a minimum depth whose measurement is limited by tip geometry. Two assemblies show smaller clefts between the two lobes and may occur on the mica at a different azimuth around the DNA axis. It is interesting that the observed fractional cleft between peaks is slightly greater than that observed for STEM mass thickness, suggesting comparable lateral resolution for biological molecules, even with present-day conventional AFM tips.

TABLE 1 Height by AFM of SV40 large T-antigen complexes bound to core origin DNA*

	Height over substrate	Length along DNA	Width ⊥ to DNA	Position on DNA‡	Midpoint position‡	n (no. of events)
	nm	nm	nm	bp	bp	
(6 + 6) mer§	15.0 ± 1.5	46 ± 8	31 ± 3	301 ± 11 to 437 ± 29	369 ± 18	8
Large partial assemblies§	12.6 ± 2.1	39 ± 2	29 ± 5	294 ± 16 to 416 ± 16	353 ± 15	13
Small partial assemblies§	10.5 ± 1.6	32 ± 5	29 ± 2	306 ± 15 to 402 ± 6	354 ± 8	8
1 mer‖	6.0 ± 0.9	20 ± 5	16 ± 3	322 ± 35 to 380 ± 23	357 ± 27	8
2–4 mer‖	9.9 ± 5.1	34 ± 8	28 ± 7	308 ± 37 to 402 ± 36	355 ± 35	5

* Entries are mean ± SD. Data are from two +ATP and one −ATP experiments using uranyl acetate.

‡ Mean length measured for the 2418-bp fragment was 793 ± 28 nm, n = 110, shorter by 4% than the 822-nm Form B length. Protein positions are given in bp, assuming 3.0 bp/nm, appropriate to Form B DNA. The sequence length from proximal fragment end to center of the core origin is 361 bp.

§ For +ATP, 35 specifically bound complexes were observed in 1 μm fields—complete assemblies (see Fig. 2*a–c*) and partial (Fig. 2*d, e*). A comparable number were scanned in 0.5-μm fields, where damage to the protein is frequently observed. Under "Large partial assemblies" we include complexes at least 12 nm in height and 35 nm in length. "Small partial assemblies" include the remaining +ATP structures. Omitted from the table is a homogeneous group of 6 single-peaked structures 50% higher than the individual peaks of the double hexamer. Similar structures are observed by STEM (unpublished data). These molecules have a natural interpretation as assemblies on end and are omitted because the meaning of the table's geometrical parameters change for such an orientation.

‖ The 8 monomers are from 13 total structures bound in the absence of ATP and observed in 1-μm fields. The remaining five structures are consistent with dimers through tetramers, which are known to bind in the absence of ATP (Mastrangelo et al., 1985).

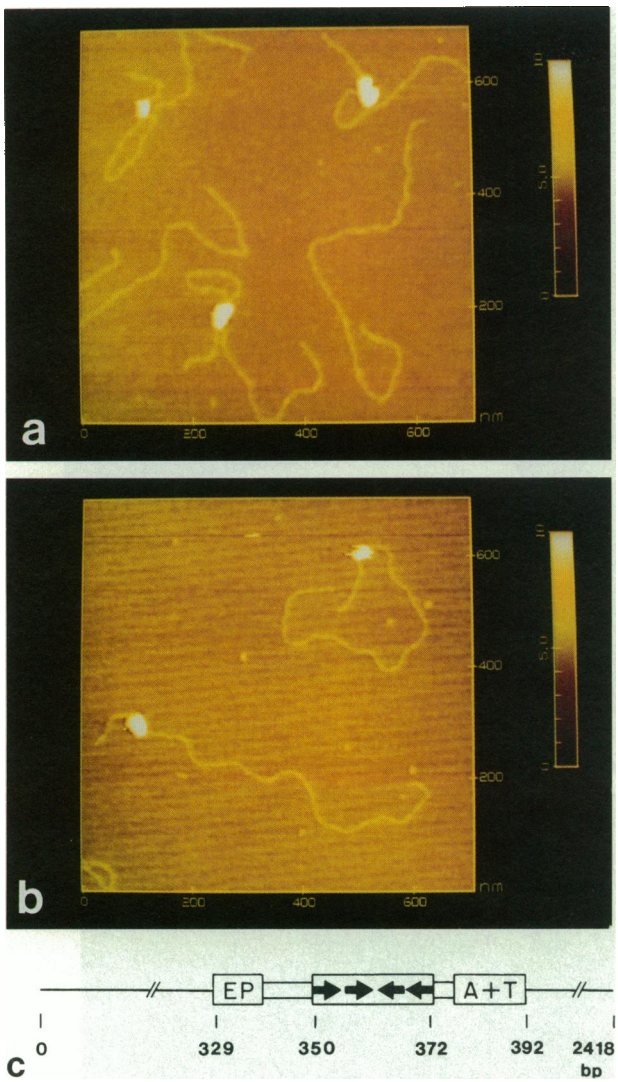

FIGURE 1 (*a*) (*b*) AFM images in top view of large T-antigen complexes at the viral origin. The white color of the complexes indicates a height more than 5 nm above the mica, set arbitrarily at 5 nm (see *color bar*). DNA is a little over 1 nm in height over mica. Displayed views are 700 × 700 nm, from 1-μm fields sampled at 400 × 400 points. Background slope has been removed. (*a*) 0° scan. (*b*) 90° scan. The apparent single-scanline flaws in the upper molecule may indicate protein damage by the tip or failure of the z servo to follow the rapid changes in height. (*c*) Diagram of linearized pOR1 vector showing the 64 bp core origin DNA that includes three essential sequence regions: the 5′-GAGGC-3′ recognition sequences (*arrows*), the AT-rich region, and the imperfect early palindrome (EP) (Deb et al., 1986). Numbers indicate distance of sites in bp from the proximal end. In the absence of ATP, up to four T-antigen monomers can bind at the 4 recognition sites, extending 65 bp along the DNA. In the presence of ATP, a hexamer assembles on each side of bp 361, covering 90 bp in all.

The overall lateral extent of the double hexamer by STEM is 30 nm × 15 nm. An excess of 8 nm on all sides is observed for AFM structures (Table 1, (6+6) mer) and is accounted for by the size of the tip. DNA is also broadened, but less so in view of its 2 nm native height. In scanning, the side of the pyramidal tip will contact convex sides of the protein surface. The shape of the tip convolutes with the shape of the protein in producing the image. Further discussion of the impact of tip geometry on AFM imaging can be found in Keller (1991).

In addition to the (6+6) mer double peaks, we also observed a second group of structures—partial assemblies composed of full-height hexamers paired with lower height oligomers (Fig. 2 *d*), and a third group—bilobed structures of reduced height, Fig. 2 *e*. Incomplete assembly had also been identified by STEM mass measurements that found one or both lobes in a bilobed structure with masses diminished by one or more monomer mass units (Mastrangelo et al., 1989). Dimensions for the three +ATP assemblies given in Table 1 show that mean height and length along the DNA both decrease, whereas lateral extent perpendicular to the DNA in the three groups remains roughly constant at 30 nm, corrected to 15 nm for tip width.

We were interested in observing complexes bound in the absence of ATP, and so to identify monomers and examine their geometrical compatibility with the double hexamer. We classified (Table 1) a homogeneous group of small molecules that bind in the absence of ATP as monomers. Three examples are shown in Fig. 3, *a–c*; the Fig. 3 *c* monomer was not stained with uranyl acetate. Among the 15 unstained complexes observed, 6 minimal structures agree with the monomers of Table 1 in lateral dimensions and height. The close similarity of the minimum structures with or without uranyl acetate treatment indicates that stain does not significantly affect protein dimensions. The asymmetric peak in the monomer profile had not been observed previously. In Fig. 3, *a* and *b* the protuberances show reversed orientation compared with Fig. 3 *c*. Opposite orientation would occur on binding to different pairs of recognition pentanucleotides that are arranged as inverted repeats.

DISCUSSION

Fig. 4 illustrates the geometrical relationship between monomers and hexamers derived from AFM height measurements. In binding reactions with and without ATP, dimethyl sulfate and DNase I protection patterns at the four pentanucleotides remain essentially unchanged, implying that T antigen interactions with DNA are equivalent (Tjian, 1979; DeLucia et al., 1983; Borowiec and Hurwitz, 1988b; Parsons et al., 1991). In the absence of ATP four monomers bind at the origin, one at each pentanucleotide. ATP then presumably alters monomer conformation to allow new protein-protein interactions: a pair of monomers bound at a pair of pentanucleotides is thought to nucleate hexamer formation around each half of the core origin (Mastrangelo et al., 1989; Dean et al., 1992). The maximal z extent of an intermediate dimer could equal the z extent of two monomers, plus DNA (Fig. 4 *c*), because specifically bound monomers bind on opposite faces of the double helix. They would occupy diametrically opposed positions in a ring hexamer. Given the addition during assembly of monomers on each side of the bound pair, the height of the completed hexamer at 15 nm is as expected with monomer plus DNA height of 5–7 nm. These topo-

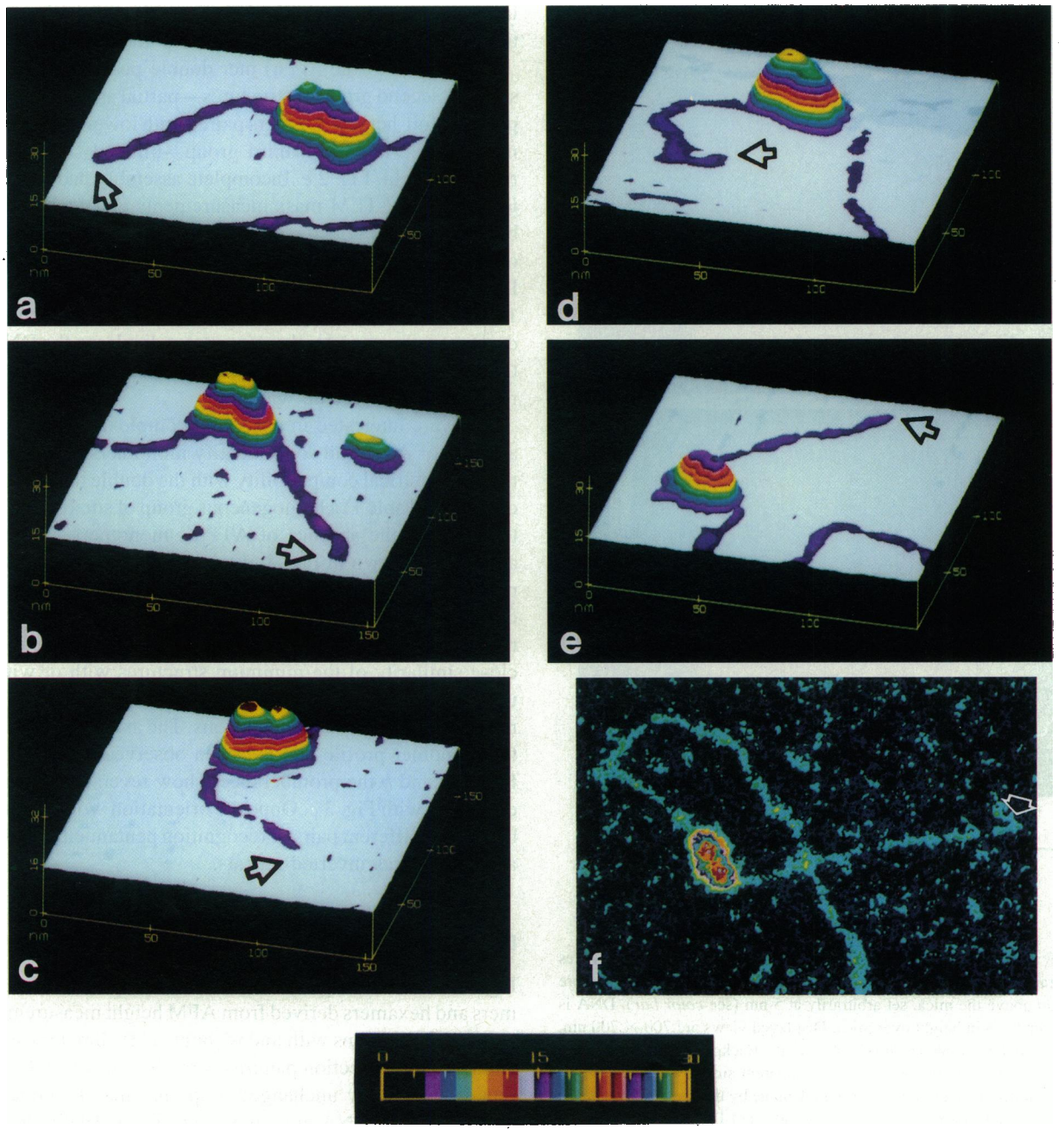

FIGURE 2 Quantitative perspective views of ATP-dependent large T antigen assemblies at core origin DNA, scanned by AFM in 1-μm fields and displayed in 150-nm subfields. The proximal DNA ends are marked by arrows. Z range is 30 or 32 nm. (*a*) (*b*) (*c*) Complete assemblies. Topography shows dual peaks of approximately equal height. Maximum heights in each assembly are 15, 13, and 14 nm. (*d*) (*e*) Incomplete assemblies. One complete and one partial hexamer (*d*), or two partials (*e*). (*f*) STEM image of the double hexamer, recorded in a 0.25-μm field and sampled at 512 × 512 data points. Displayed subfield is 170 × 130 nm, magnification 1.3 × AFM (*a–e*). Color coding indicates scattered electron counts, proportional to mass per nm^2.

graphical measurements provide the first geometrical evidence for the structural relationships of monomers in the replication assembly. The overall model was derived by STEM molecular mass measurement and confirmed by detection of 1 through 6 protein-DNA bands on nondenaturing polyacrylamide gels (Parsons et al., 1991; Dean et al., 1992).

AFM height measurements may be combined with STEM two-dimensional projected mass distributions to estimate mass density in space for the T antigen double hexamer. At the centers of each T antigen hexamer, projected onto the support plane, STEM mass per nm^2 attains a maximum of 6600 Da/nm^2 as determined by scattered electron counts (Mastrangelo et al., 1989). Combining this value with 15 nm, the maximum AFM z coordinate, gives 440 Da/nm^3 as the maximum value for mass per unit volume averaged through the protein along a line perpendicular to the substrate. This value is low compared to the 840 ± 50 Da/nm^3 obtained from the partial specific volumes, 0.68–0.78 cm^3/g, characteristic

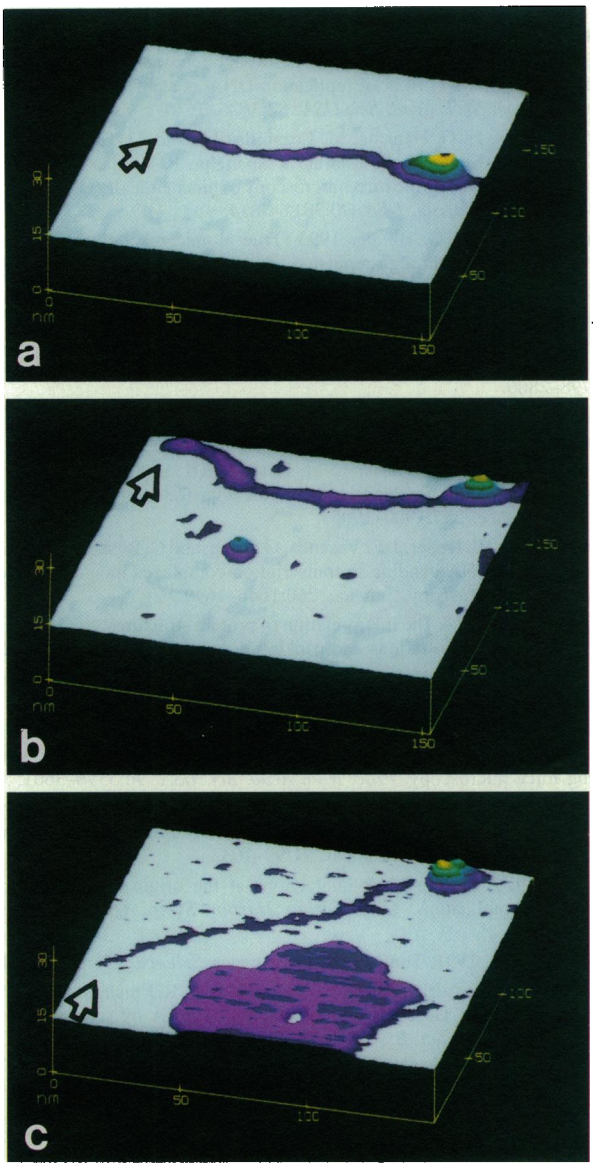

FIGURE 3 Smallest T-antigen subunits bound to origin DNA in the absence of ATP. This group, whose dimensions are given in Table 1, is taken to be the monomer structure. Z range is 30 nm. Arrows point to proximal ends of DNA. (*a*) (*b*) Uranyl acetate stain was applied as for the +ATP structures shown in Figs. 1 and 2. (*c*) This subunit is representative of a homogeneous group of six structures observed in preparations not treated with uranyl acetate. Average height of the unstained DNA is, at 0.5 nm, half of that in *a* and *b*. The large flat contaminant has not been identified.

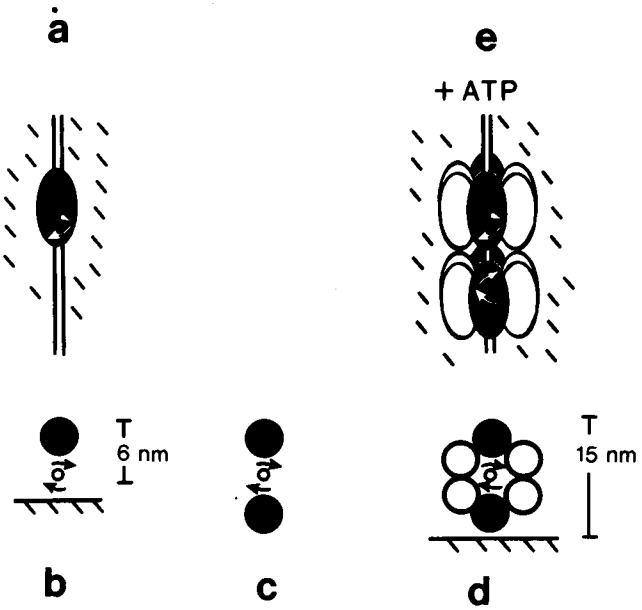

FIGURE 4 Drawing represents how a monomer subunit 5 nm in height can assemble into a 15 nm high hexamer. Upper, top view; lower, end view. (*a*) (*b*) A monomer binds at one pentanucleotide recognition site, represented by a curved arrow. (*c*) Monomers bind at both sites in half of the central palindrome. In the presence of ATP, monomers at the two sites undergo an allosteric change in conformation that allows formation of (*d*) a hexamer and (*e*) double hexamer, at two and four recognition sites, respectively.

of many proteins. Richards showed that, for several crystallized monomeric proteins, average density over the envelope volume determined by x-ray diffraction is only slightly less (perhaps 5–10%) than the partial specific volume value (Richards, 1974). Thus, the low average density of 440 Da/nm^3 for the T antigen double hexamer based on AFM height is suggestive of an internal void in the structure, and it is in adequate agreement with the approximately 2/3× partial-specific-volume density expected from Fig. 4.

If atomic resolution can be achieved, AFM should contribute valuable surface-structural data for modeling protein-DNA and protein-protein interactions. Identification of the macromolecules involved may be increasingly possible. In EM, the noise caused by statistical fluctuation in number of scattered electrons is evident and, when the target structure is available only in low copy number, leads to a requirement for a dose of incident electrons that destroys order at the atomic level. In AFM of biological molecules, it is not clear yet what resolution will ultimately be obtainable. It is clear that the force on protein by the tip must be carefully limited, and it is likely that obtaining the necessary low force requires scanning in solution, at least for unstained preparations (Persson, 1987; Ohnesorge and Binning, 1993). Certainly, Ohnesorge and Binnig's recent demonstration of true atomic-scale lateral resolution in the surface profile of crystalline $CaCO_3$ as scanned under fluid encourages the quest for extension to protein and DNA.

This work was supported by the U. S. Department of Energy, Office of Health and Environmental Research (to I. A. Mastrangelo and P. V. C. Hough), by grants from the U. S. National Science Foundation (DIR 9018846 to H. G. Hansma), and by Digital Instruments, Inc.

REFERENCES

Binnig, G., C. F. Quate, and C. Gerber. 1986. Atomic force microscope. *Phys. Rev. Lett.* 56:930–933.

Borowiec, J. A., F. B. Dean, P. A. Bullock, and J. Hurwitz. 1990. Binding and unwinding–how T antigen engages the SV40 origin of DNA replication. *Cell.* 60:181–184.

Borowiec, J. A., and J. Hurwitz. 1988a. ATP stimulates the binding of

simian virus 40 (SV40) large tumor antigen to the SV40 origin of replication. *Proc. Natl. Acad. Sci. USA.* 85:64–68.

Borowiec, J. A., and J. Hurwitz. 1988b. Localized melting and structural changes in the SV40 origin of replication induced by T-antigen. *EMBO J.* 7:3149–3158.

Bustamante, C., J. Vesenka, C. L. Tang, W. Rees, M. Guthold, and R. Keller. 1992. Circular DNA molecules imaged in air by scanning force microscopy. *Biochemistry.* 31:22–26.

Dean, F. B., J. A. Borowiec, T. Eki, and J. Hurwitz. 1992. The simian virus 40 T antigen double hexamer assembles around the DNA at the replication origin. *J. Biol. Chem.* 267:14129–14137.

Dean, F. B., M. Dodson, H. Echols, and J. Hurwitz. 1987. ATP-dependent formation of a specialized nucleoprotein structure by simian virus 40 (SV40) large tumor antigen at the SV40 replication origin. *Proc. Natl. Acad. Sci. USA.* 84:8981–8985.

Deb, S., A. L. DeLucia, C. P. Baur, A. Koff, and P. Tegtmeyer. 1986. Domain structure of the simian virus 40 core origin of replication. *Mol. Cell. Biol.* 6:1663–1670.

Deb, S. P., and P. Tegtmeyer. 1987. ATP enhances the binding of simian virus 40 large T antigen to the origin of replication. *J. Virol.* 61: 3649–3654.

DeLucia, A. L., B. A. Lewton, R. Tjian, and P. Tegtmeyer. 1983. Topography of simian virus 40 A protein-DNA complexes: arrangement of pentanucleotide interaction sites at the origin of replication. *J. Virol.* 46: 143–150.

Fanning, E., and R. Knippers. 1992. Structure and function of simian virus 40 large tumor antigen. *Ann. Rev. Biochem.* 61:55–85.

Hansma, H. G., J. Vesenka, C. Siegerist, G. Kelderman, H. Morrett, R. L. Sinsheimer, V. Elings, C. Bustamante, and P. K. Hansma. 1992. Reproducible imaging and dissection of plasmid DNA under liquid with the atomic force microscope. *Science.* 256:1180–1184.

Hayat, M. A. 1980. Principles and Techniques of Electron Microscopy, Biological Applications. University Park Press, Baltimore, MD. 522 pp.

Keller, D. 1991. Reconstruction of STM and AFM images distorted by finite-size tips. *Surface Science.* 253:353–364.

Lyubchenko, Y. L., B. L. Jacobs, and S. M. Lindsay. 1992. Atomic force microscopy of reovirus dsRNA: a routine technique for length measurements. *Nucleic Acids Res.* 20:3983–3986.

Mastrangelo, I. A., P. V. Hough, J. S. Wall, M. Dodson, F. B. Dean, and J. Hurwitz. 1989. ATP-dependent assembly of double hexamers of SV40 T antigen at the viral origin of DNA replication. *Nature.* 338:658–662.

Mastrangelo, I. A., P. V. Hough, V. G. Wilson, J. S. Wall, J. F. Hainfeld, and P. Tegtmeyer. 1985. Monomers through trimers of large tumor antigen bind in region I and monomers through tetramers bind in region II of simian virus 40 origin of replication DNA as stable structures in solution. *Proc. Natl. Acad. Sci. USA.* 82:3626–3630.

Murray, M. N., H. G. Hansma, M. Bezanilla, T. Sano, D. F. Ogletree, W. Kolbe, C. L. Smith, C. R. Cantor, S. Spengler, P. K. Hansma, and M. Salmeron. 1993. Atomic force microscopy of biochemically tagged DNA. *Proc. Natl. Acad. Sci. USA.* 90:3811–3814.

Ohnesorge, F., and G. Binnig. 1993. True atomic resolution by atomic force microscopy through repulsive and attractive forces. *Science.* 260: 1451–1455.

Parsons, R. E., J. E. Stenger, S. Ray, R. Welker, M. E. Anderson, and P. Tegtmeyer. 1991. Cooperative assembly of simian virus 40 T-antigen hexamers on functional halves of the replication origin. *J. Virol.* 65: 2798–2806.

Persson, B. N. J. 1987. The atomic force microscope: can it be used to study biological molecules? *Chem. Phys. Lett.* 141:366–368.

Radmacher, M., R. W. Tillmann, M. Fritz, and H. E. Gaub. 1992. From molecules to cells: imaging soft samples with the atomic force microscope. *Science.* 257:1900–1905.

Rees, W. A., R. W. Keller, J. P. Vesenka, G. Yang, and C. Bustamante. 1993. Evidence of DNA bending in transcription complexes imaged by scanning force microscopy. *Science.* 260:1646–1649.

Richards, F. M. 1974. The interpretation of protein structures: total volume, group volume distributions and packing density. *J. Mol. Biol.* 82:1–14.

Rugar, D., and P. K. Hansma. 1990. Atomic force microscopy. *Physics Today.* 43:23–30.

Samori, B., G. Siligardi, C. Quagliariello, A. L. Weisenhorn, J. Vesenka, and C. J. Bustamante. 1993. Chirality of DNA supercoiling assigned by scanning force microscopy. *Proc. Natl. Acad. Sci. USA.* 90:3598–3601.

Shaiu, W. L., D. D. Larson, J. Vesenka, and E. Henderson. 1993. Atomic force microscopy of oriented linear DNA molecules labeled with 5nm gold spheres. *Nucleic Acids Res.* 21:99–103.

Tjian, R. 1979. Protein-DNA interactions at the origin of simian virus 40 DNA replication. *Cold Spring Harbor Symp. Quant. Biol.* 2: 655–661.

Weinberg, R. A. 1991. Tumor suppressor genes. *Science.* 254:1138–1146.

Zenhausern, F., M. Adrian, B. ten Heggeler-Bordier, R. Emch, M. Jobin, M. Taborelli, and P. Descouts. 1992. Imaging of DNA by scanning force microscopy. *J. Struct. Biol.* 108:69–73.